Miner Deposita (2006) 41: 1–16
DOI 10.1007/s00126-005-0035-5

ARTICLE

H. Albert Gilg · Maria Boni · Giuseppina Balassone · Cameron R. Allen · David Banks · Farid Moore

Marble-hosted sulfide ores in the Angouran Zn-(Pb–Ag) deposit, NW Iran: interaction of sedimentary brines with a metamorphic core complex

Received: 5 August 2005 / Accepted: 1 November 2005 / Published online: 10 February 2006

Abstract The Angouran Zn-(Pb–Ag) deposit, Zanjan Province, NW Iran, is located within the central Sanandaj-Sirjan Zone of the Zagros orogenic belt. The deposit has proven and estimated resources of 4.7 Mt of sulfide ore at 27.7% Zn, 2.4% Pb, and 110 g/t Ag, and 14.6 Mt of oxidized carbonate ores at 22% Zn and 4.6% Pb. It is hosted by a metamorphic core complex that is unconformably overlain by a Neogene volcanic and evaporite-bearing marine to continental sedimentary sequence. The sulfide orebody, precursor to the significant nonsulfide ores, is located at the crest of an open anticline at the contact between Neoproterozoic to Cambrian footwall micaschists and hanging wall marbles. ^{40}Ar–^{39}Ar data on muscovite from mineralized and unaltered footwall micaschists suggest a rapid Mid-Miocene exhumation of the metamorphic basement (~20 Ma) and yield an upper age constraint for mineralization. The fine-grained sulfide ore is massive, replacive, often brecciated, clearly postmetamorphic and dominated by Fe-poor sphalerite, with minor galena, pyrite, anhydrite, quartz, muscovite, dolomite, and rare calcite. Sphalerite contains Na–Ca–Cl brine inclusions (23–25 mass% total dissolved solids) with homogenization temperatures of 180–70°C. Fluid inclusion chemistry (Na–K–Li–Ca–Mg–Cl–Br), ore geochemistry, S, and Pb isotope data suggest that the Angouran sulfide ore formed by the interaction of modified, strongly evaporated Miocene seawater and the lithotypes of an exhumed metamorphic core complex. Minor contributions of metals from Miocene igneous rocks cannot be excluded. Mineralization occurred in a collisional intra-arc setting with high heat flow, probably during the transition from an extensional to a compressional regime. The Angouran deposit may represent a new type of low-temperature carbonate-hosted Zn–Pb ore that is distinct from Mississippi Valley type and sedimentary-exhalative deposits.

Editorial handling: B. Lehmann

H. A. Gilg (✉)
Lehrstuhl für Ingenieurgeologie,
Technische Universität München,
Arcisstr. 21,
80290 Munich, Germany
e-mail: agilg@tum.de
Tel.: +49-89-28925855
Fax: +49-89-28925852

M. Boni
Dipartimento Geofisica & Vulcanologia,
Università di Napoli,
Naples, Italy

M. Boni
Geologisch-Paläontologisches Institut,
Universität Heidelberg,
Heidelberg, Germany

G. Balassone
Dipartimento Scienze della Terra,
Università di Napoli,
Naples, Italy

C. R. Allen
Teck Cominco American,
Spokane, WA, USA

D. Banks
School of Earth Sciences,
University of Leeds,
Leeds, UK

F. Moore
Geological Department,
University of Shiraz,
Shiraz, Iran

Introduction

The Angouran Zn-(Pb–Ag) deposit is located in western Zanjan Province, Iran, about 90 km west of Zanjan and 450 km northwest of Tehran (Fig. 1a). The deposit is presently the largest producer of zinc in Iran, and it is a world-class, high-grade nonsulfide Zn deposit with a significant, but yet unexploited, sulfide orebody. Ore resources were estimated in 1999 at 14.6 Mt of nonsulfide ore at 22.6% Zn and 4.6% Pb, and 4.7 Mt of sulfides at 27.7% Zn, 2.4% Pb, and 110 g/t Ag based on a cut-off grade of 4% Zn (Annels et al. 2003).

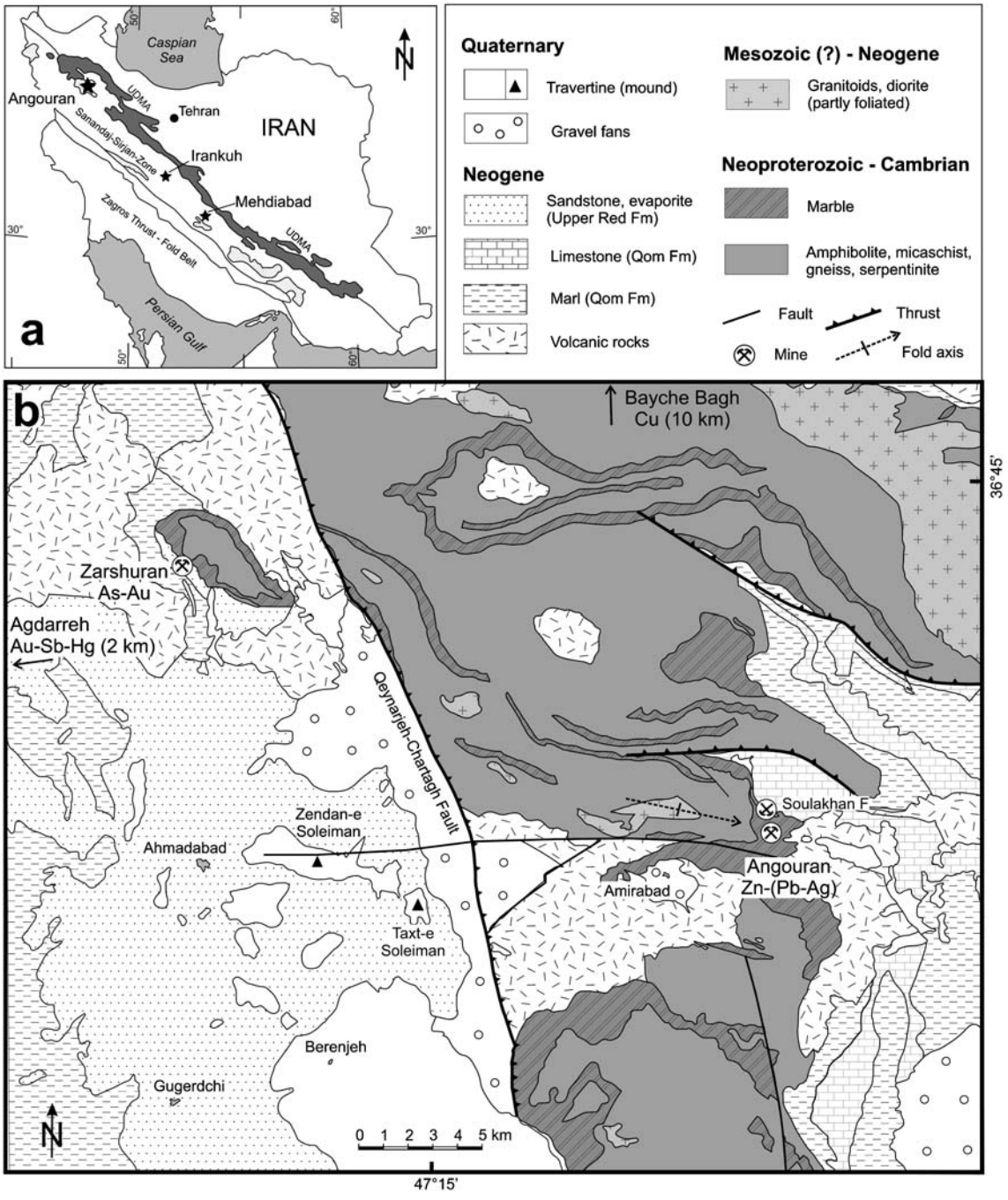

Fig. 1 **a** Location of the Angouran and other Iranian Zn–Pb deposits (Irankuh, Mehdiabad) in the central Zagros orogenic belt. Hatched areas represent metamorphic basement complexes within the Sanandaj-Sirjan Zone. *UDMA*, Urumieh-Dokhtar Magmatic Arc. **b** Schematic regional geological map of the Takab-Zanjan area, NW Iran, based on Babakhani and Ghalamghash (1990)

The first historic account of Au, Ag, Hg, Pb, and orpiment mining in the Takab area, near the ancient town of Shiz (probably the present Taxt-e Soleiman archeological site 20 km west of Angouran), was given by Abu-Dulaf Mis'ar ibn Muhalhil, an Arabian writer in the tenth century A.D. (Minorskij 1955). Houtum-Schindler (1881) mentioned for the first time underground lead (cerussite) mining activities both at Angouran, alternative spellings "Anguran" or "Angooran," and in the nearby, now abandoned, fluorite mines of Soulakhan. Zinc mining started at Angouran after World War II, and production increased with the development of an open pit in 1963 (Bariand et al. 1965). The first geological and mineralogical descriptions of the marble-hosted Angouran Zn-(Pb–Ag) deposit were presented by Burnol (1968) and Hirayama (1968). Hirayama considered the sulfide orebody as being formed by metasomatic, structurally controlled replacement processes with a postmetamorphic emplacement age. He remarked that the sulfides, though located between two metamorphic units, were devoid of any metamorphic over-

print. Hirayama assigned a supergene origin to the Zn carbonate ores. Very little geological work has been published since then on the deposit (e.g. Alinia 1989; Haditsch 1990).

Recently, due to renewed interest in nonsulfide mineralization throughout the world, the Angouran deposit became the object of new scientific research (Annels et al. 2003; Borg and Daliran 2004; Daliran and Borg 2003; Maanijou 2002; Gilg and Boni 2004; Gilg et al. 2003; Sadeghi 2003). The main results of this research are the prevalence of genetic models of postmetamorphic emplacement of the sulfides as opposed to that of a premetamorphic Proterozoic volcanogenic massive sulfide (VMS)-type mineralization (Maanijou 2002). The sulfides were ascribed either to a sedimentary-exhalative (SEDEX) process during the Mesozoic (Annels et al. 2003), to the effects of a distal intrusion-related hydrothermal system (Daliran and Borg 2003; Borg and Daliran 2004), or to deposition from Ca-rich brines similar to Mississippi Valley type (MVT) deposits (Gilg et al. 2003). However, with the sole exception of Gilg et al. (2003), the economically most significant part of the deposit, consisting of Zn carbonates, has been considered as being a product of exclusively supergene processes (Borg and Daliran 2004; Daliran and Borg 2003; Hitzman et al. 2003).

Other ore deposits in the region (Asadi and Hale 2001) include the Soulakhan occurrence, a small smithsonite-bearing fluorite–barite–calcite vein system located 500 m north of the Angouran pit; the Zarshuran As–Au and Agdarreh Au–Sb–Hg deposits (Asadi et al. 1999; Daliran et al. 2002; Mehrabi et al. 1999); and the Ni–Co–As–Bi-bearing Bayche–Bagh Cu vein mineralization (Ladame 1945; Lotfi and Karimi 2004).

In this study, we present the geological setting, ore petrography, and new geochemical data, including ^{40}Ar–^{39}Ar geochronological data, fluid inclusions, and S and Pb isotope data, to constrain the origin of sulfide ores at Angouran. A companion paper will focus on the origin of the nonsulfide carbonate ores at Angouran and advocates a hypogene origin for most of the Zn carbonate ore that are presently mined.

Geological setting

In contrast to other large Iranian Zn–Pb deposits such as Irankuh and Mehdiabad that are hosted by Lower Cretaceous limestones, the Angouran deposit is located within one of a number of metamorphic inlier complexes in the central Sanandaj-Sirjan Zone of the Zagros orogenic belt, close to the Urumieh-Dokhtar Magmatic Arc (Fig. 1a). The Zagros belt formed as a consequence of Tertiary continental collision between the Afro-Arabian plate and smaller Gondwana-derived microplates, after subduction of the Neotethys ocean during the Cretaceous (e.g., Alavi 1994; Glennie 2000). The crystalline rocks in the Takab-Zanjan area comprise a series of amphibolites, gneisses, mica-schists, serpentinites, and marbles affected by greenschist to amphibolite faces metamorphic conditions (Gazanfari 1991, unpublished master's thesis). The lithotypes are interpreted to represent a metamorphosed intraoceanic island arc complex (Gazanfari 1991, unpublished master's thesis). Recent zircon U/Pb dating of a granitic gneiss from the Maneshan area suggests a Pan-African intrusion age (about 560 Ma) of the protolith (Stockli et al. 2004). Hamdi (1995) reports on the occurrences of Early Cambrian fossils (e.g., *Latouchella* sp., *Bemella* sp., and *Halkiera stenobasis*) in marbles near Amirabad. Thus, a Neoproterozoic–Cambrian age of the basement rocks seems highly probable. The deformation of these basement rocks is complex, with internal top-to-the-southwest-directed thrusting, isoclinal folding, and a superimposed open folding with E-W striking fold axes. The timing of metamorphism and deformation is not well constrained.

The crystalline rocks are unconformably overlain by volcanic and marine to continental sedimentary rocks of (Oligo?-)Miocene age. This Late Paleogene to Early Neogene sedimentation period within the orogen is related to a phase of intra-arc extension with rapid exhumation of basement rocks as metamorphic core complexes along low-angle detachment faults (Stockli et al. 2004). The post-metamorphic lithological sequence starts with a continental clastic series of red sandstones, conglomerates, and gypsiferous marls, corresponding to the Lower Red Formation, which outcrops only marginally in the Angouran area. The Lower Red Formation is followed by intermediate to predominantly silicic pyroclastic rocks (ignimbrites and tuffs) and minor lava flows, subvolcanic dikes, and shallow intrusive stocks. The tuffs display a local pervasive clayey alteration (illitization) in the area of the Angouran mine camp. The volcanic rocks and, locally, the metamorphic rocks are overlain by Miocene shallow marine limestones corresponding to the Qom Formation. These consist mainly of pack stones with abundant echinoderm fragments, red corallinacean algae, *acervulinidae*, and minor bryozoa and *rotalidae*. The limestones are succeeded by a several-hundred-meters-thick continental series of evaporite-bearing red marls, sandstones, and conglomerates (equivalents of the Upper Red Formation). These Upper Miocene gypsum-bearing red beds host Iran's largest borate deposit at Gharah Gol, approximately 20 km SE of Angouran (Rahimpour-Bonab and Kazemi 2003), several smaller halite and potash deposits (e.g., Duzkhand, Khareh Naz, Sidler, Iljaq, and Qarah-Aghaje; Rahimpour-Bonab and Kalantarzadeh 2005), and the small sulfur deposits of Gugerdchi (Damm 1968). At its western border, the previously mentioned metamorphic complex has been thrust westward over the Miocene volcanic and sedimentary rocks along the Qeynarjeh-Chartagh Fault (Fig. 1b), indicating a compressional regime during the Late Neogene (Pliocene) (Stockli et al. 2004). This compressive tectonic regime is responsible for significant uplift and mountain building (the Angouran deposit is located almost 3,000 m above sea level), and the high levels of seismic activity in the region (e.g. Houtum-Schindler 1881).

The Quaternary strata consist of significant travertine deposits, gravel fans, and recent alluvium. Hot-spring-derived carbonate deposits are widespread in the region and form the extensive travertine field of Berenjeh, smaller

patches of travertine outcropping east of Zarshuran, the Taxt-e Soleiman mound, the 110-m-high, impressive cone of Zendan-e Soleiman (Naumann 1961; Damm 1968), and a flat-lying bedded travertine plateau, 500 m east of the Angouran mine, here referred to as the Angouran mine camp travertine (Fig. 1b). Currently active, carbonate-depositing thermal springs (20–45°C) occur between Taxt-e Soleiman and Ahmedabad as part of the NW Takab geothermal field.

Geometry and zoning of the orebodies

The geometry of the Angouran mineralized zone is complex. In plan view, the orebody, comprising both sulfide and carbonate ores, is some 600 m in length, with an N–S orientation, and 200–400 m across. It is situated in the crest of an open anticlinal structure within the metamorphic basement that plunges eastward at 10–20° (Fig. 1b). The ore zone is bounded by NNW–SSE, NW–SE, and NE–SW trending faults. The sulfide orebody is more or less tabular, restricted to the lithological boundary between micaschists in the footwall and fine-grained calcite marbles in the hanging wall and is overlain by nonsulfide Zn ores (Fig. 2). Various ore types are distinguished by mine geologists in the Angouran deposit and given here in italics.

Sulfide ores are replacive, semiconcordant to strongly discordant to the host rocks, and accompanied by no obvious wall rock alteration. The sulfide orebody dips to the south, reaching its maximum thickness of more than 50 m at the southern end of the ore zone (Fig. 2). It grades downwards into mineralized schists containing only minor discordant sulfide mineralization and barren micaschists. The sulfide body is capped by a mushroom-shaped zone of up to 200-m-thick Zn carbonate ores, which protrude discordantly into the marble of the hanging wall (Fig. 2).

Mixed sulfide carbonate ore occurs at the contact between sulfide and nonsulfide ores and rarely within the nonsulfide ores. A variety of Zn carbonate or "oxide" ore types occurs throughout the deposit. The textures are variably soft and earthy (*soft carbonate ore*), hard and botryoidal to crustiform (*hard carbonate ore* and *calamine ore*), multiply brecciated (*breccia carbonate ore*), and cavernous with abundant open space and voids. They will be described in more detail in a companion paper. Both sulfide and carbonate ore types are closely associated with a wide variety of breccias, especially along the three main fault zones, which define the lateral limit of the deposit.

Methods

Minerals were characterized by optical microscopy, scanning electron microscopy (SEM; Jeol JSM-5310), and X-ray powder diffraction (XRD) analysis (Seifert MZVI and Philips PW1800 automated diffractometer, CuKα radiation). Major element analysis of selected samples was performed by energy-dispersive spectroscopy (EDS; Link Analytical 10,000, ZAF corrections). Silicates, oxides, and pure elements were used as standards, and the operating conditions were 15 kV acceleration voltage and 10 μm spot size.

Microthermometric measurements of fluid inclusions were carried out using a United States Geological Survey

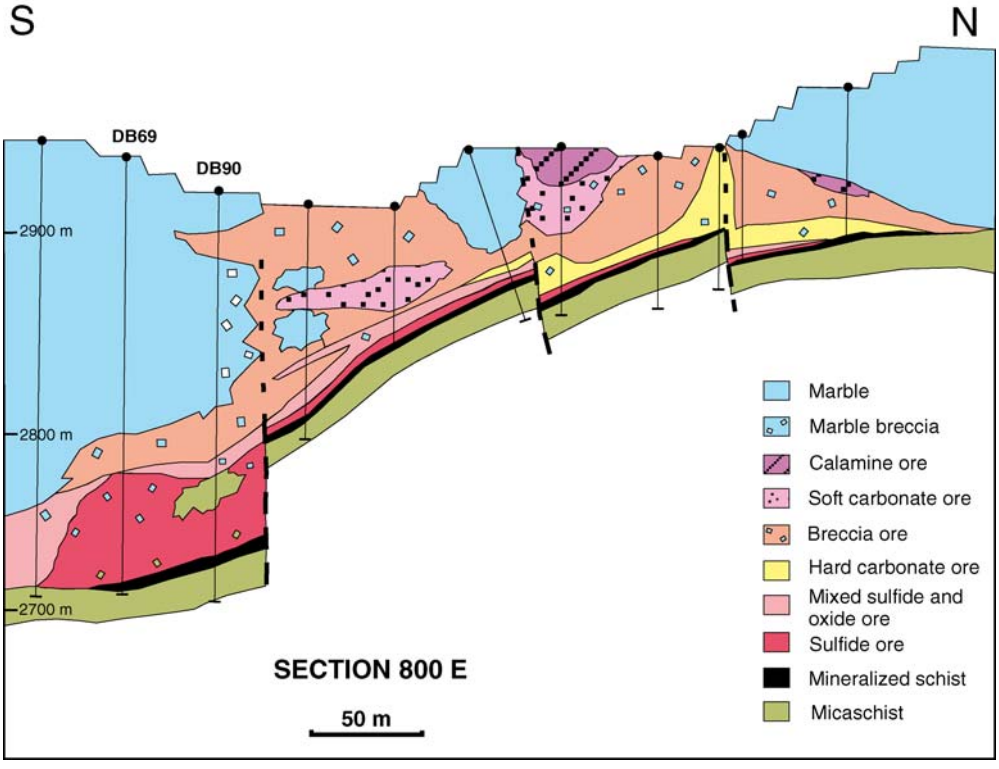

Fig. 2 Geological N–S section through the Angouran orebody at 800 E with two drill cores (DB69 and DB90). The sulfide ore is located at the contact of footwall micaschists and hanging wall marbles and reaches maximum thickness in the south. Elevation in meters above sea level

(USGS) heating/freezing stage at the Geological Survey of Canada, Quebec, and a Linkam THMSG 600-TMS 93 heating/freezing stage at Technische Universität München, calibrated using synthetic fluid inclusions. The precision of measurements is ±0.1°C between −60 and +40°C and ±1°C above +40°C. Chemical analysis of the fluid inclusions in different minerals was carried out using the bulk crush-leach method as detailed in Banks et al. (2000). The samples were crushed to between 1 and 2 mm grain size, boiled several times in 18.2 MΩ water, and dried prior to analysis. Approximately 0.5–1 g of material was crushed, transferred to a suitable container, and leached with 18.2 MΩ water for anion and Na, K, and Li analysis or $LaCl_3$ solution for Ca and Mg. Anions were analyzed by ion chromatography, Na, K, and Li were analyzed by flame emission spectroscopy, and all cations were analyzed by inductively coupled plasma–mass spectrometry (ICP-MS). Replicate analyses show the precision to be on average 5% relative standard deviation for the analysis of these samples.

Sulfur isotope values of sulfides ($\delta^{34}S_{CDT}$) were determined on hand-picked mineral separates at the Isotope Science Laboratory, Dept. of Physics and Astronomy, Calgary, Canada, using a continuous flow elemental analyzer (Carlo Erba NA 1500) attached to a VG Prism II mass spectrometer. Analytical precision is better than 0.7‰.

Pb isotope ratios were determined at the Radiogenic Isotope Facility of the University of Alberta, Edmonton, Canada. After extraction of Pb using HBr-HNO_3 anion exchange chromatography, the Pb isotope ratios were measured using a VG MM30 mass spectrometer operating in a single collector mode.

The ^{40}Ar–^{39}Ar analyses were performed at the New Mexico Geochronology Research Laboratory at the New Mexico Institute of Mining and Technology. Mineral separates were prepared using standard crushing, heavy liquid, and hand-picking techniques. Separated material from fine-grained samples R0011539 and R009323 was individually sealed in evacuated quartz tubes, while sample R0010672 was loaded into a machined Al disk. Samples were irradiated for 100 (R0011539 and R009323) or 24 h (R0010672) along with interlaboratory standard Fish Canyon tuff sanidine FC-1 (27.84 Ma) as a neutron flux monitor in L-67 position (Ford Memorial Reactor, University of Michigan). Encapsulation tubes were punctured with a 50 W CO_2 laser to allow trapped gas to be analyzed. The samples were step-heated in a Mo double-vacuum resistance furnace attached to an automated all-metal extraction line. Reactive gases were removed by reaction with SAES GP-50 getters operated at 450 and 20°C. Isotope ratios were measured using a Mass Analyzer Products 215-50 mass spectrometer operated in electron multiplier mode with an overall sensitivity of 7.0×10^{-17} mol Ar/pA. The extraction system and mass spectrometer blanks and backgrounds were measured throughout the course of the analysis and were reproducible and corrected for. All errors are reported at the 2σ confidence level, and decay constants and isotopic abundances are from Steiger and Jäger (1977). The total gas age and error were calculated by weighting individual steps by the fraction of ^{39}Ar released. Plateau ages were calculated for contiguous heating steps that have apparent ages yielding mean-squared weighted deviation (MSWD) values that are within the predicted 95% confidence interval for $n-1$ degrees of freedom and by weighting each step by the inverse variance. If the MSWD is above the 95% confidence window, the plateau error is multiplied by the square root of the MSWD.

Petrography and paragenesis of the sulfide ores

The sulfide ores are generally fine-grained, massive, and often have breccia texture containing highly angular clasts of micaschists and marbles, as well as fragments of sulfide ore, indicating that multiple brecciation events occurred during mineralization (Fig. 3a–d). The dominant ore mineral (60–75 vol%) is dark red to yellowish Fe-poor

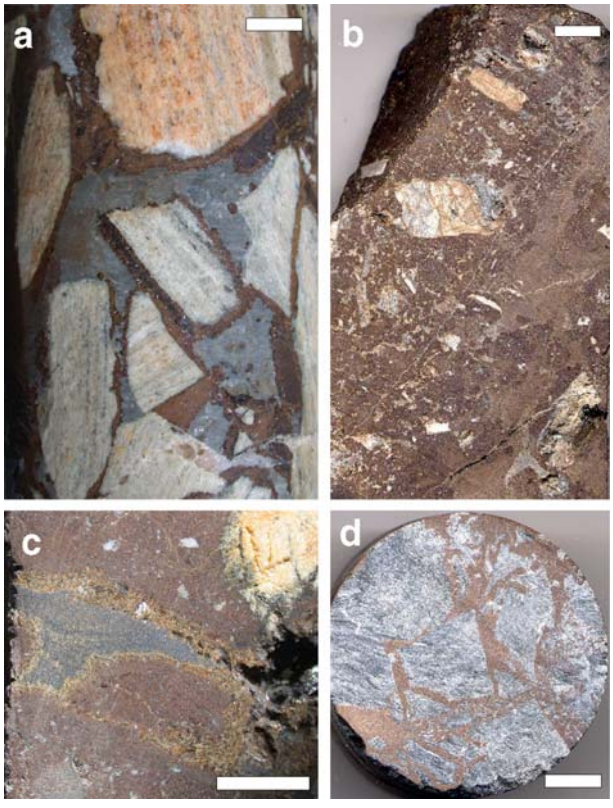

Fig. 3 Photographs of sulfide ore textures from Angouran (scale bar in all pictures=1 cm). **a** Breccia with angular foliated marble and micaschist fragments cemented by brownish sphalerite and a fine-grained siliceous matrix (drill core DB69, 179.4 m). **b** Brecciated sulfide ore with small marble and micaschist clasts. Note brecciation of dark early sphalerite ore and cementation with a lighter sphalerite generation at the left side of the picture (drill core DB90, 184 m; B4). **c** Late honey brown sphalerite rim on early dark red-brown sphalerite ore clast with fine-grained siliceous ore matrix (drill core DB90, 196.3 m) **d** Sphalerite-cemented breccia of footwall micaschists (drill core DB90, 180.5 m; B5)

sphalerite, commonly displaying complex oscillatory zoning (Fig. 4b) with no signs of a metamorphic overprint. Two main generations of sphalerite can be distinguished (Fig. 3c, 4b): an early fine-grained, red-brown sphalerite and a late oscillatory-zoned honey yellow sphalerite. Subordinate Sb-bearing galena, rare anhedral pyrite (Fig. 4c), and traces of Ni–Co arsenides exclusively found as micrometer-sized inclusions in quartz (Fig. 4d) complete the paragenesis of the sulfide ores. Daliran and Borg (2003) also recorded in the sulfide ores arsenian pyrite and undetermined Pb–As–Sb sulfosalt minerals. The gangue minerals are generally sparse (<40 vol%) and comprise euhedral quartz (<100 μm), muscovite flakes (Fig. 4f), rare sparry calcite, rhombohedral dolomite (Fig. 4e), and tabular anhydrite, often as relic ghost textures (Fig. 4a,e). The latter two minerals have only been detected enclosed in sphalerite. Anhydrite (and/or barite?) was apparently originally quite abundant in sulfide ores (locally up to approximately 30 vol%) but has been almost completely dissolved, leaving tabular cavities (relic ghost textures) that are now partly filled with later-stage ore minerals (euhedral galena and smithsonite). The common occurrence of euhedral galena crystals lining the cavities of former anhydrite crystals (Fig. 4g) documents a phase of sulfide precipitation following anhydrite dissolution. It is not clear whether this phase of galena precipitation is related to the late stage of sulfide ore formation or to the superimposed carbonate ore formation. Almost all sulfide ore samples show some variable degree of Zn carbonate mineralization, as infill of cavities and fractures, or as replacement of gangue minerals, marble clasts, and sulfides, indicating that Zn carbonate ore formation has pervasively overprinted sulfide ore. Thus, a continuum between sulfide ores, mixed sulfide-carbonate ores, and Zn carbonate ores can be observed. This smithsonite-forming overprint has obliterated the contact between sulfide ores and hanging wall marbles.

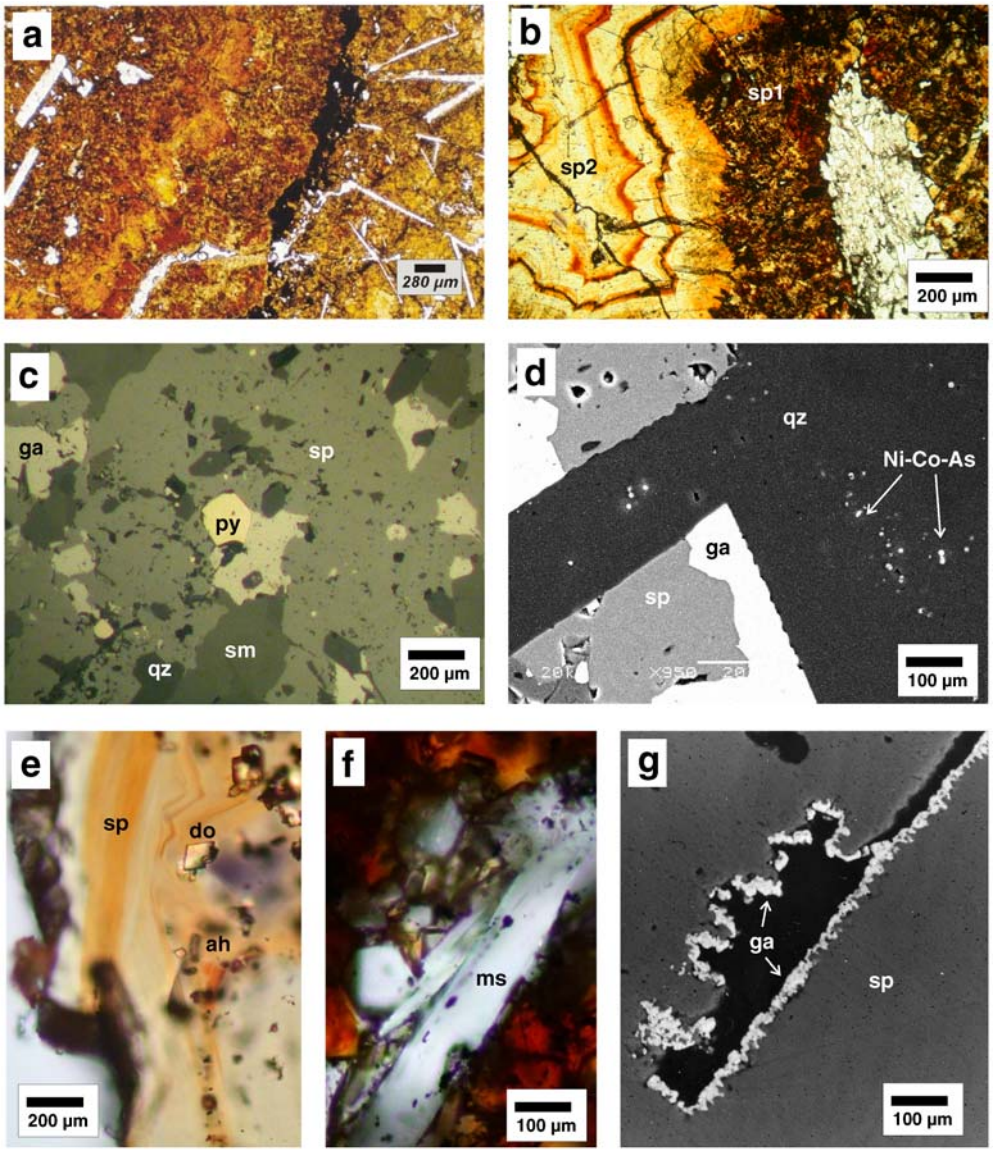

Fig. 4 Microphotographs of sulfide ores from Angouran. **a** Sphalerite-rich ore with lath-shaped pseudomorphs of polycrystalline smithsonite aggregates after anhydrite. **b** Early dark red-brown sphalerite (*sp1*) and late oscillatory-zoned honey sphalerite (*sp2*) with marble clast (drill core DB69, 234 m). **c** Reflected light microphotograph of sulfide ore with sphalerite (*sp*), galena (*ga*), pyrite (*py*), quartz (*qz*), and smithsonite (*sm*) (DB69, 218.7 m). **d** Backscattered electron image of Ni–Co–As-rich inclusions in euhedral quartz (*qz*) with sphalerite (*sp*) and galena (*ga*) (drill core DB69, 234 m). **e** Syngenetic inclusions of rhombohedral dolomite (*do*) and lath-shaped anhydrite (*ah*) in growth zone of late honey sphalerite (*sp*) (drill core DB69, 218.7 m). **f** Muscovite (*ms*) with syngenetic sulfide inclusions in sulfide ore (drill core DB69, 234 m). **g** Late galena (*ga*) rim in cavity of dissolved toothbrush-shaped anhydrite in sphalerite (*sp*) (drill core DB90, 200 m)

Chemistry of the sulfide ores

The sulfide ores are generally characterized by a very high Zn content (>35 wt%) and generally low Pb content (<3 wt %). The average trace element composition of 21 sulfide ore samples reveals high Ag (210 ppm), As (760 ppm), Sb (300 ppm), Hg (20 ppm), Co (400 ppm), and Ni (344 ppm) contents, and low Cu (250 ppm), Mn (350 ppm), and Au (<0.01 ppm).

Fluid inclusions

Abundant fluid inclusions are present in early dark-brown and late yellowish sphalerite (Fig. 5a–c). They range in size from less than 2 up to 20 μm, often display negative crystal or rounded isometric shapes, and occur mostly as isolated inclusions, often along growth zones but rarely in clusters. They are mainly primary in origin, with only a few considered as pseudosecondary or secondary. The inclusions contain two phases, a colorless aqueous liquid and small vapor bubble, at room temperature and have a consistent degree of fill [$V_{LIQ}/(V_{LIQ}+V_{VAP})$=0.95]. Only very rarely was necking observed. The results of microthermometric measurements are shown in Fig. 6. The sphalerite-hosted inclusions have very low first-melting temperatures (between about −30 and −50°C, mostly around −40°C), indicating the presence of significant amounts of divalent cations, most probably Ca^{2+} (and/or Mg^{2+}), in addition to NaCl. Ice-melting temperatures are similar for early and late sphalerite, ranging from −18.1 to −28.4°C, but mainly cluster between −21 and −25°C. Due to the poor transparency of sphalerite, we could not accurately measure hydrohalite melting prior to ice melting. A few measurements yielded low hydrohalite melting temperatures of less than −25°C, indicating chloride-dominated fluids rich in divalent cations such as Ca^{2+} (Oakes et al. 1990). We found no evidence for the formation clathrates during freezing runs, indicating low contents of gases such as carbon dioxide or methane. Homogenization temperatures range from 162 to 125°C for early sphalerite and from 140 to 73°C for late sphalerite (Fig. 6). These results indicate that Ca-rich chloride brines with relatively constant and high salinities of 21–25 mass% total dissolved salts were the fluids responsible for sphalerite mineralization. We find no evidence for mixing of fluids with variable salinities. The temperatures of sulfide precipitation appear to decrease during deposition from the early dark to late honey sphalerite. The pressure corrections of the homogenization temperatures are estimated at less than 50°C (Zhang and Frantz 1987), as the maximum overburden during mineralization probably did not exceed 1–2 km.

Fluid inclusions in fluorite samples from the small Soulakhan fluorite–barite vein deposit have very similar microthermometric characteristics to those of the nearby Angouran sulfide ores. Preliminary microthermometric

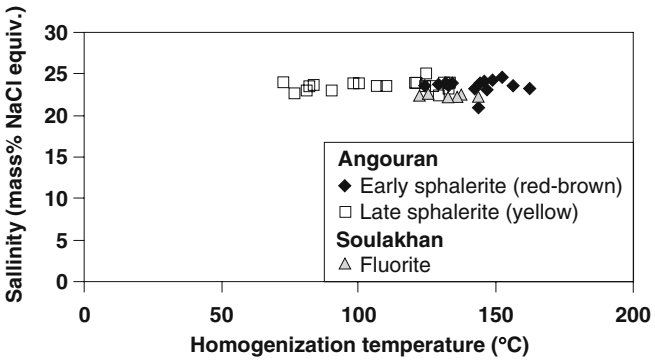

Fig. 6 Results of microthermometry of early and late sphalerite from Angouran sulfide ores and fluorite from Soulakhan vein deposit

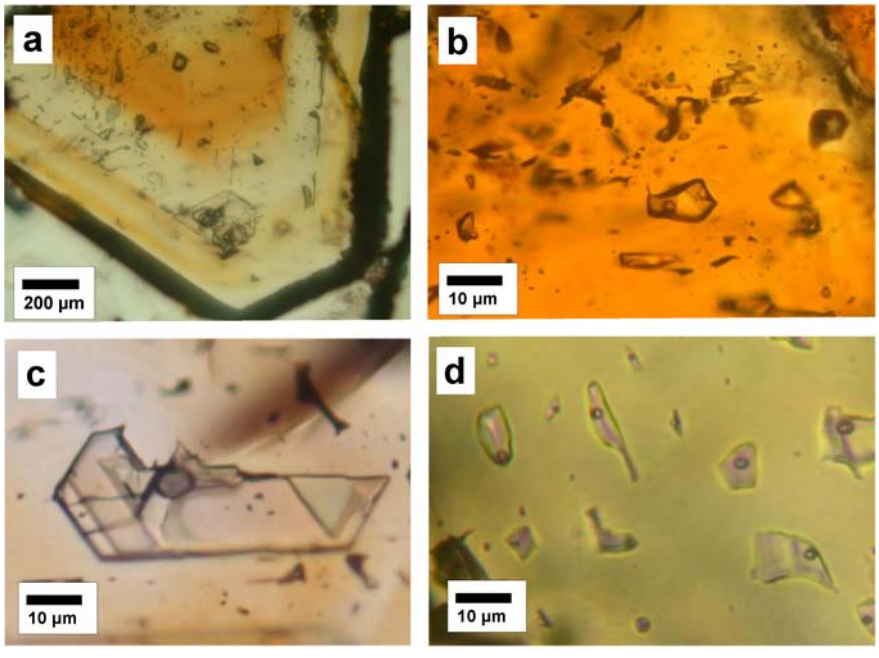

Fig. 5 Microphotographs of fluid inclusions. **a** Primary fluid inclusions in growth zones of late sphalerite from Angouran (drill core DB69, 234 m). **b** Group of liquid-rich two-phase inclusions in early red-brown sphalerite from Angouran (drill core DB69, 234 m). **c** Large primary two-phase inclusion in growth zone of late honey sphalerite, Angouran (drill core DB69-234 m). **d** Group of secondary two-phase inclusions in fluorite from Soulakhan (sample A21)

studies on two-phase liquid-rich inclusions mostly of pseudosecondary and secondary origin (Fig. 5d) indicate low first-melting temperatures (−52°C) and last-melting temperatures of −20°C. The homogenization temperatures vary between 139 and 123°C (Fig. 6). Similar results were reported by Sadeghi (2003).

The results of crush-leach analyses of three sphalerite samples and a sparry calcite from Angouran and a fluorite sample from Soulakhan are given in Table 1. The crush-leach analyses confirm the microthermometry results of an Na–Ca–Cl-dominated composition of inclusion fluids with a molar $CaCl_2$/(NaCl + $CaCl_2$) of approximately 0.5. Elemental ratios (e.g., Na/K, Na/Ca, Na/Li, Na/Mg, Br/Cl, and F/Cl) are very similar for the analyzed samples from Angouran and Soulakhan, indicating a relatively homogeneous and similar mineralizing fluid. The low molar Cl/Br ratios (164–228) are indicative of brines originating from highly evaporated seawater, i.e., beyond the point of halite saturation, although minor admixture of halite dissolution brines cannot be excluded (e.g., Grandia et al. 2003; Viets et al. 1996; Walter et al. 1990). We note that Cl/Br ratios of diverse magmatic hydrothermal fluids (e.g., Böhlke and Irwin 1992; Banks et al. 2000) are generally much higher than those reported here for the Angouran and Soulakhan deposits. Na/Br and Cl/Br ratios (Fig. 7a) show that the fluids are consistent with evaporation of seawater well past halite saturation and almost to the point where epsomite precipitates. All the data from the sphalerite-hosted inclusions lie on or close to the evaporation trajectory, indicating that little loss of Na due to water–rock interaction has taken place. However, inclusions in calcite and fluorite do lie left of the seawater evaporation line, suggesting some loss of Na. The fact that Cl and Br are conservative in solution (except where dissolution or precipitation is involved) can be used to constrain the starting composition of the ore fluid prior to water–rock interaction. In Fig. 7, the Na, K, and Li concentration of fluid inclusions has been recalculated using a salinity of 25 mass% determined from microthermometry and the crush-leach analyses. Relative to the evaporation trend of seawater (Fontes and Matray 1993), the sphalerite-hosted fluid inclusions plot on the evaporation trend, toward the end of halite precipitation, exactly at the position that is required by their Cl/Br ratios. While this does not preclude some gain or loss of Na and/or K from the evaporated seawater, it does not suggest a significant change from the concentrations expected for seawater evaporated to this degree. However, the fluid inclusions in fluorite and calcite have lower Na and K concentrations than expected. The concentrations of Na and K are approximately half the expected values, and in this instance, indicate significant modification by fluid–rock interaction. In contrast, Li concentrations of inclusions in sphalerite, calcite, and fluorite are enriched relative to the expected concentrations in seawater evaporated to this degree; thus, Li has been gained by fluid–rock interaction.

At this degree of evaporation, seawater should contain no Ca and high concentrations of Mg. In fact, the opposite is the case here. The low molar Mg/Cl (0.012–0.015) and high Ca/Cl (0.19–0.23) ratios suggest significant modification of the divalent element concentrations of the evaporated seawater by fluid–rock reactions such as dolomitization, chloritization, illitization, or albitization (e.g., Viets et al. 1996; Grandia et al. 2003).

The application of various cation geothermometers (Kharaka and Mariner 1989; Verma and Santoyo 1997) to the fluid inclusion leachate data from Angouran and Soulakhan yields conflicting results. Sphalerite-hosted inclusions give temperatures between 250 and 300°C based on Na/K, but temperatures about 50°C lower based on Na/Li (Verma and Santoyo 1997). The Mg/Li thermometer (Kharaka and Mariner 1989) yields consistent, but even much lower, temperatures of about 100°C, broadly consistent with fluid inclusion homogenization temperatures. The calculated temperatures of calcite- and fluorite-hosted inclusions using the Na/K and Na/Li geothermometer (Verma and Santoyo 1997) are between 300 and 350°C. The Na/K geothermometer is known to yield anomalously high temperatures in Ca-rich waters, especially at low temperatures (Kharaka and Mariner 1989). The calcite- and fluorite-hosted inclusions have lost Na as compared to the sphalerite-hosted inclusions (Fig. 7c) and thus yield higher temperatures using the Na/Li geothermometer. Thus, we suggest that the results of Na/Li and Mg/Li thermometry on sphalerite-hosted inclusions (240–100°C) may give the most reliable maximum temperature estimate for fluid–rock equilibration.

Table 1 Fluid inclusion crush-leach data (in parts per million, recalculated to a salinity of 25 mass% NaCl as determined from the microthermometry of the fluid inclusions)

Sample		F	Cl	Br	Na	K	Li	Ca	Mg
Angouran									
Sphalerite	DB69, 218 m	1,124	151,630	1,674	45,826	9,561	40	32,883	1,515
Sphalerite	DB69, 234 m	376	151,630	2,089	39,666	10,542	35	33,702	1,279
Sphalerite	Open pit (AT7)	965	151,630	2,040	39,279	6,404	42	39,658	1,503
Calcite	Open pit (A34)	NA	151,630	1,583	26,242	6,805	46	NA	NA
Soulakhan									
Fluorite	Open pit (A21)	NA	151,630	1,500	18,456	5,767	63	NA	NA

NA Not analyzed because of contamination from the host mineral

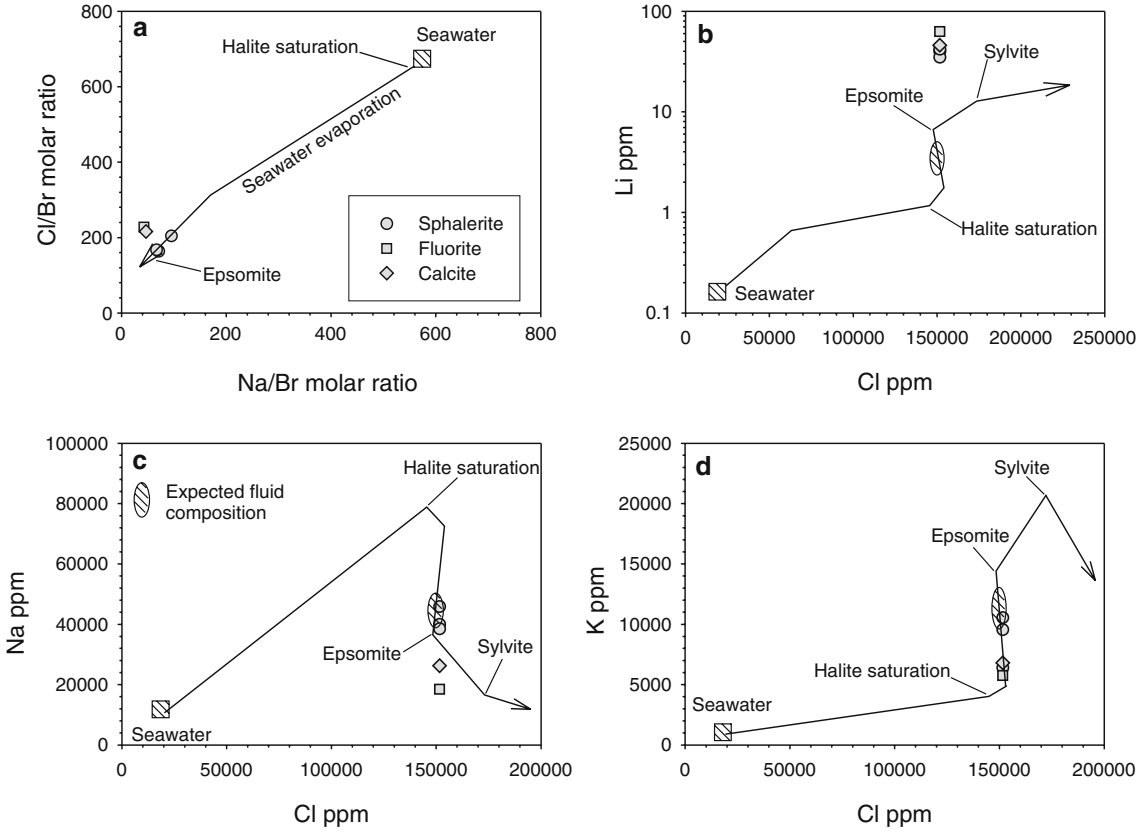

Fig. 7 **a** Cl/Br and Na/Br ratios of the fluid inclusions relative to the evaporation trend for modern seawater. The fluids are highly evaporated almost to epsomite saturation. Fluid inclusions in sphalerite are exactly on the evaporation trend, showing that little Na loss for the fluid has occurred during fluid–rock interaction. The fluids in fluorite and calcite plot to the *left*, indicating that significant amounts of Na have been lost. **b**–**d** The calculated Li, Na, K, and Cl concentrations relative to the seawater evaporation trend. Inclusions in sphalerite have exactly the Na and K concentrations expected for the degree of evaporation estimated from the Cl/Br ratios. Fluid inclusions in fluorite and calcite have significantly less Na and K than expected. Li in fluid inclusions is strongly enriched relative to evaporated seawater

S and Pb isotope data

Preliminary sulfur isotope data (Table 2) on early dark-brown sphalerite, late honey sphalerite, and galena from the sulfide ores show a rather restricted range of $\delta^{34}S$ values from 5.2 to 8.0‰ (n=8). Early sphalerite is isotopically slightly lighter than late sphalerite from the same sample. The overall range of isotope values of both sphalerite generations is overlapping. The sulfur isotope values at Angouran are higher than the values of typical magmatic sulfur (0±5‰, Ohmoto and Goldhaber (1997), suggesting a nonmagmatic (sulfate?) source of sulfur. The isotope values are not compatible with bacterial reduction of Miocene marine seawater sulfate but suggest thermochemical sulfate reduction (e.g., Machel et al. 1995; Ohmoto and Goldhaber 1997). We note that the sulfur isotope values are similar to those from the MVT-type deposit of Reocín, Spain (Velasco et al. 2003). The sulfur isotope data of Angouran contrast with the sulfur isotope compositions of sphalerite from the Irankuh deposit (−9.6 to −3.6‰) reported by Ghazban et al. (1994).

Reconnaissance Pb isotope data (n=3) from both sulfide and carbonate ores from Angouran are homogeneous and cluster around values of $^{206}Pb/^{204}Pb$=18.922±2, $^{207}Pb/^{204}Pb$=15.700±3, and $^{208}Pb/^{204}Pb$=38.908±9. A single galena value from

Table 2 Sulfur isotope data

Mineral, description	Location (drill hole)	$\delta^{34}S_{CDT}$ (‰)
Sphalerite, early, dark red-brown	DB55b, 128.9 m	6.9
Sphalerite, early, dark red-brown	DB69, 181.6 m	8.0
Sphalerite, early, dark red-brown	DB69, 186.25 m	6.7
Sphalerite, late, honey brown	DB69, 186.25 m	7.3
Sphalerite, early, dark red-brown	DB90, 194.5 m	5.2
Sphalerite, late, honey brown	DB90, 194.5 m	7.4
Galena, very late	DB90, 194.5 m	7.6
Sphalerite, black	Bench 2, open pit	7.8

Table 3 ^{40}Ar–^{39}Ar step-heating data of muscovites from unmineralized (R0011539) and mineralized footwall micaschist (R0010672), and a sericite–kaolinite sample from sulfide ores (R009323)

ID	Temperature (°C)	$^{40}Ar/^{39}Ar$	$^{37}Ar/^{39}Ar$	$^{38}Ar/^{39}Ar$ ($\times10^{-3}$)	$^{39}Ar_K$ ($\times10^{-15}$ mol)	K/Ca	^{40}Ar* (%)	^{39}Ar (%)	Age (Ma)	±1σ (Ma)
R0011539 (muscovite, wt=17.68 mg), *J*=0.0038210, NM-136, lab number=52164-10										
AAA encapsulation		14.58	0.1036	44.99	35.0	4.93	8.7	2.2	8.7	8.7
A	550	6.563	0.0129	17.61	6.91	39.7	20.3	2.7	9.13	0.50
B	600	4.274	0.0097	5.856	14.5	52.8	59.0	3.6	17.20	0.26
C	650	3.766	0.0033	3.22	6.55	157	74.3	4.0	19.05	0.27
D	675	3.362	0.0033	1.629	41.2	169	85.3	6.6	19.499	0.072
E	700	3.191	0.0027	0.895	48.3	192	91.3	9.7	19.810	0.060
F	730	3.119	0.0018	0.4055	70.2	279	95.8	14.1	20.309	0.050
G	760	3.056	0.0016	0.2129	97.8	310	97.6	20.3	20.263	0.042
H	800	3.035	0.0017	0.1287	154	296	98.4	30.1	20.294	0.040
I	840	3.027	0.0018	0.1048	133	291	98.6	38.5	20.285	0.038
J	860	3.026	0.0016	0.1062	211	329	98.6	51.9	20.272	0.039
K	900	3.033	0.0014	0.1084	261	363	98.6	68.4	20.321	0.034
L	1,000	3.068	0.0014	0.1139	411	366	98.5	94.5	20.544	0.042
M	1,200	3.233	0.0128	0.3934	45.9	39.8	96.2	97.4	21.137	0.059
N	1,650	3.455	0.0367	0.4202	40.3	13.9	96.1	100.0	22.588	0.060
Total gas age (*n*=15)					1,576	298			20.07	0.60[c]
Plateau[a] (*n*=7; steps F-L)					1,338	335		84.9	20.32	0.05[c]
R0010672 (muscovite, wt=1.07 mg), *J*=0.0158733, NM-134, lab number=52095-01										
A	600	2.0100	0.0747	3.858	4.32	6.83	42.8	6.7	24.1	1.5
B	650	1.2440	0.0137	0.7694	2.90	37.3	81.0	11.2	28.0	2.0
C	700	0.9754	0.0099	1.1215	2.96	51.7	61.7	15.8	16.7	1.7
D	775	0.8963	0.0095	0.4473	6.61	54.0	84.2	26.0	20.9	0.67
E	825	0.8420	0.0063	0.2221	6.51	81.5	91.2	36.1	21.22	0.73
F	875	0.8199	0.0040	0.1163	7.89	129	94.8	48.4	21.47	0.63
G	900	0.8139	0.0038	0.552	4.81	136	78.5	55.9	17.6	1.2
H	925	0.8274	0.0051	0.5261	3.39	99.4	79.8	61.1	18.3	1.4
I	975	0.8260	0.0053	0.212	3.69	96.9	91.4	66.9	20.9	1.3
J	1,010	0.8671	0.0044	−0.1007	3.62	115	102.8	72.5	24.6	1.4
K	1,050	0.8316	0.0023	0.2563	4.20	226	89.8	79.0	20.6	1.3
L	1,110	0.8207	0.0019	0.2999	9.51	266	88.0	93.7	19.96	0.58
M	1,300	1.6920	0.0243	2.618	3.28	21.0	58.1	98.8	27.5	1.7
N	1,650	19.7500	0.1695	42.63	0.75	3.01	36.2	100.0	194	11.0
Total gas age (*n*=14)					64.45	117			23.4	2.4[c]
Plateau[b] (*n*=10; steps C-L)					53.20	137		82.6	20.6	0.56[c]
ROO 9323 (sericite, wt=16.21 mg), *J*=0.0038222, NM-136, lab number=52165-02										
AAA encapsulation		30.09	0.0451	97.75	16.7	11.3	3.9	13.0	8.1	1.0
A	550	15.4000	0.0486	36.80	38.4	10.5	29.2	42.8	30.71	0.46
B	600	6.4090	0.0441	6.472	28.7	11.6	69.9	65.1	30.49	0.18
C	650	6.5630	0.0587	6.071	17.5	8.69	72.4	78.7	32.34	0.26
D	675	6.9230	0.0633	6.900	8.09	8.05	70.3	85.0	33.13	0.37
E	700	7.7340	0.0445	8.779	5.92	11.5	66.2	89.6	34.85	0.65
F	730	8.3990	0.0588	10.11	5.46	8.67	64.2	93.8	36.7	1.1
G	760	8.3500	0.0479	10.02	4.09	10.6	64.3	97.0	36.54	0.64
H	800	9.3050	0.0604	13.2	3.88	8.45	57.9	100.0	36.65	0.76
Total gas age (*n*=9)					129	10.4			28.9	1.0[c]
No plateau										

[a]MSWD=1.3
[b]MSWD=1.2
[c]2σ errors

the Soulakhan deposit has very similar Pb isotope ratios ($^{206}Pb/^{204}$ Pb=18.985, ^{207} Pb/^{204}Pb=15.699, and ^{208} Pb/^{204} Pb=38.772), indicating a common Pb source for the fluorite vein deposit and the large Angouran Zn-(Pb–Ag) deposit. These isotope ratios are indicative of an upper crustal source with a high U/Pb ratio and give a Cenozoic model age using the growth curves of the plumbotectonics model (Doe and Zartman 1979). In the absence of Pb isotope data of possible source rocks in the region, a further discussion of the Pb isotope data is not warranted. It is notable, however, that the ores of the Angouran deposit are characterized by more radiogenic Pb than Iranian Zn–Pb deposits hosted in Cretaceous carbonate rocks such as Irankuh and Mehdiabad (Lancelot et al. 1997), and are with respect to uranogenic lead identical to the Jabali deposit, Yemen (Al Ganad et al. 1994).

^{40}Ar–^{39}Ar geochronology

Three samples were selected for ^{40}Ar–^{39}Ar geochronology: a muscovite separate from an unaltered footwall biotite-bearing quartz–muscovite schist (R0011539; outside the pit), a muscovite separate from weakly mineralized and hydrothermally altered footwall quartz–muscovite schist from the open pit (R0010672), and a sericite-bearing kaolinite-rich clayey material (R009323) from the matrix of a sphalerite-bearing breccia (drillhole DH69, 179.8 m). The results are presented in Table 3 and Fig. 8. The muscovite from the unaltered footwall schists (R0011539) has a well-behaved ^{40}Ar–^{39}Ar age spectrum with a weighted mean "plateau" age of 20.32±0.05 Ma calculated from seven steps covering approximately 84% of ^{39}Ar released during heating (MSWD=1.3). This plateau age is indistinguishable within error from the total gas age (20.07± 0.60 Ma) and is interpreted as a cooling age (~350±50°C; Purdy and Jäger 1976) during Early Miocene exhumation of the metamorphic basement. The muscovite sample of the altered micaschist (R0010672) has a much more disturbed saddle-shaped age spectrum (Fig. 8). A plateau age of 20.56±0.56 Ma was calculated for ten steps (C–L) covering about 83% of the ^{39}Ar released. The inverse isochron plot ($^{39}Ar/^{40}Ar$ vs $^{36}Ar/^{40}Ar$; not shown here) shows significant scatter (MSWD=5, n=14), with an apparent isochron age of 19.4±4.4 Ma and a $^{40}Ar/^{36}Ar$ intercept of 420±50. The high $^{40}Ar/^{36}Ar$ intercept and the saddle-shaped age spectrum suggests the presence of excess or extraneous ^{40}Ar. However, the plateau age is within error identical to the muscovite age of the unaltered micaschist, suggesting that the temperatures during mineralization were not high enough to reset the K–Ar system of muscovite, i.e., they were below about 350±50°C. The fine-grained sericite-bearing matrix from a sulfide ore breccia (R009323) yields a strongly disturbed staircase-shaped spectrum (Fig. 8c) with an integrated total age of 28.9± 1.0 Ma. No plateau age could be calculated. The integrated age is much higher than the cooling ages of muscovites from the metamorphic wall rocks. This observation strongly suggests the presence of excess ^{40}Ar in the fine-grained mica related to sulfide mineralization. Thus, the geochronological data only give an upper age constraint on the mineralization of about 20 Ma.

Criticism of earlier genetic concepts

The presence of rotated clasts of marble and micaschists in sulfide ore, crosscutting relationships of mineralized veins with respect to the schistosity of the metamorphic host rocks, the existence of delicately zoned sphalerite with large primary fluid inclusions with no textural evidence of reequilibration, and the absence of ductile deformation textures in sulfides are clear evidence for a postmetamorphic origin of the sulfide ores (Gilg et al. 2003; Daliran and Borg 2003, 2005). Thus, a syngenetic, premetamorphic origin for the Angouran sulfide ores (e.g., Haditsch 1990; Maanijou 2002) is not supported by our observations. Our geochronological data constrain the timing of uplift and exhumation of the metamorphic host rocks at Angouran and thus yield a maximum age for the mineralization (Mid-Miocene, ~20 Ma). This age, the presence of Cambrian fossils (Hamdi 1995), and a clear metamorphic schistosity in the Angouran marbles also conflict with the recently proposed genetic model of Annels et al. (2003), who suggest that the host carbonate rocks at Angouran are Mesozoic limestones that were converted to marble ("marbleized") during Mesozoic syngenetic exhalative mineralization. Our observations show that the Zn-(Pb–Ag) mineralization at Angouran is clearly epigenetic and postmetamorphic.

The fluid inclusion data indicate that the Angouran Zn ores and the nearby fluorite veins of Soulakhan formed from Ca- and Br-rich brines at temperatures of less than 200°C. There is no microthermometric evidence for the presence of gases such as CO_2 or CH_4, fluid immiscibility (boiling), and mixing with low-salinity fluids. Many of these features of the ore-forming fluid contrast with those that are characteristic of high-temperature carbonate-hosted replacement deposits (CRDs) related to igneous activity (e.g., Gilg 1996; Megaw 1998) but are rather similar to sedimentary or shield brines. The Angouran ores are devoid of the ferroan and manganoan carbonates that typify CRD deposits. In order to evaluate the possibility of a direct genetic link for Angouran mineralization and the regional Miocene andesitic to rhyolitic magmatic activity, as suggested by Daliran and Borg (2003) and Borg and Daliran (2004), we compare the fluid and geochemical characteristics of Angouran sulfide ores with those of other deposits in the region that are possibly related to Miocene igneous activity: the Zarshuran As–Au deposit (Asadi et al. 1999; Daliran et al. 2002; Mehrabi et al. 1999) and the Bayche–Bagh Cu–Pb–Zn–Ni–Co–As–Bi deposit (Ladame 1945; Lotfi and Karimi 2004). The Carlin-type Zarshuran As–Au deposit is hosted by Precambrian black shales and marbles (Chaldagh unit) above the greenschists and serpentinites (Imam–Kahn unit) that form a small dome structure within the Upper Red sandstones (Fig. 1b). The As–Au mineralization is rich in pyrite (partly As-rich) and arsenic sulfides (orpiment and realgar), but it also

contains minor stibnite, sphalerite, galena, various sulfosalts, cinnabar, tellurides (coloradoite), and rare thallium minerals (e.g., lorandite and galkhaite) in a gangue of quartz, calcite, and sericite, locally also barite and fluorite (Asadi et al. 1999; Mehrabi et al. 1999). K–Ar and ^{40}Ar–^{39}Ar dating indicate that this epigenetic and postmetamorphic mineralization is coeval with Miocene volcanic activity (~14.2±0.4 Ma; Mehrabi et al. 1999). Fluid inclusion studies indicate mixing of a deep CO_2±CH_4-rich fluid of magmatic (or metamorphic?) origin, with meteoric groundwater and ore deposition between 260 (main stage) and 180°C (late stage) at a depth of at least 3.8±1.8 km (Mehrabi et al. 1999). The Bayche–Bagh Cu–Pb–Zn–Bi–Co–Ni–As vein deposit in the northern part of Takab Quadrangle is hosted by Miocene rhyolites that overlie the Precambrian basement with gneisses and amphibolites (Ladame 1945; Lotfi and Karimi 2004). Fluid inclusion homogenization temperatures are between 210 and 470°C, with salinities of approximately 25 mass% NaCl equiv. (Lotfi and Karimi 2004).

In conclusion, the Fe-, Cu-, and Au-poor character and the rather simple mineralogy of the sulfide mineralization at Angouran, as well as the fluid composition and the much lower temperatures of ore formation, do not favor a direct genetic link with Miocene igneous activity and magmatic fluids. A preliminary survey of fluid inclusions in quartz phenocrysts of the altered rhyolitic tuffs and a subvolcanic granodiorite in the Angouran area did not reveal the presence of Na–Ca–Cl brines.

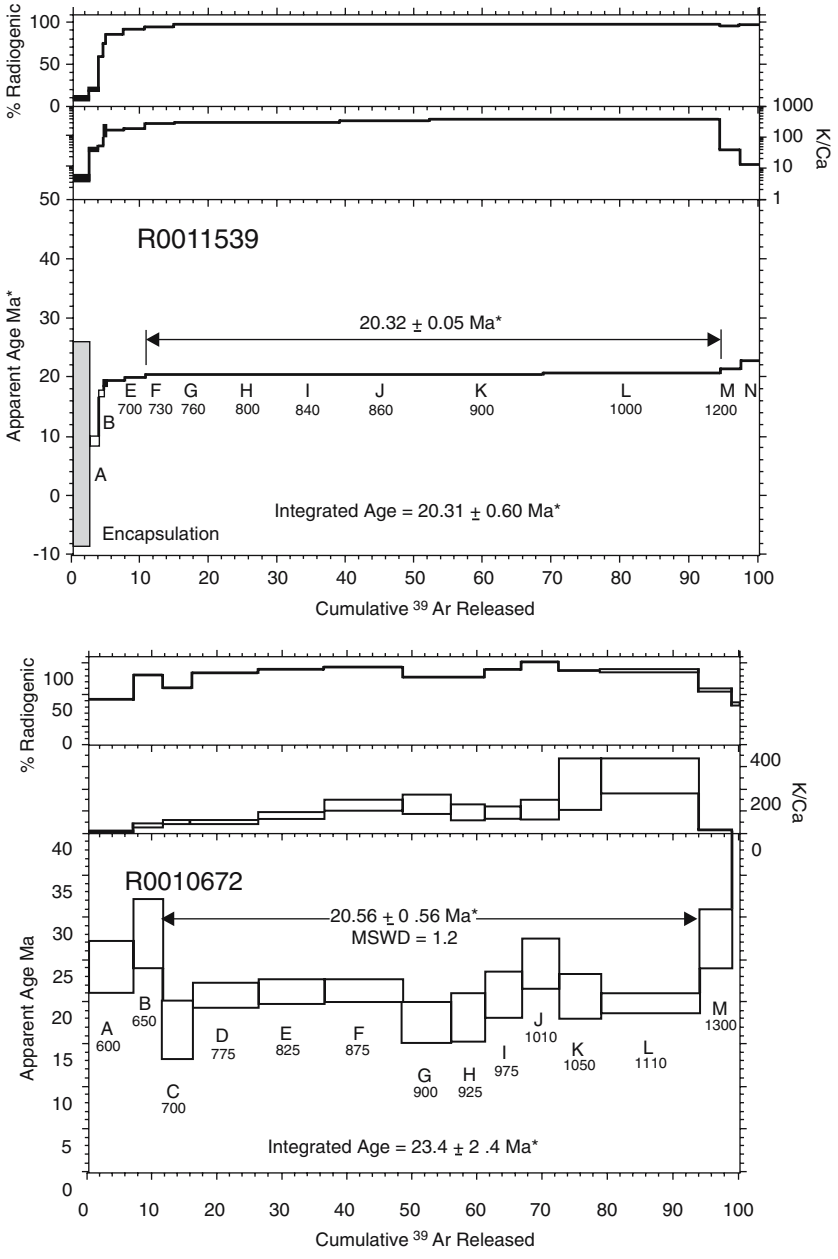

Fig. 8 ^{40}Ar–^{39}Ar age spectra, K/Ca, and radiogenic yield diagrams for muscovites from unmineralized (R0011539) and mineralized schist (R0010672), and a sericite–kaolinite sample from sulfide ores (R009323). Encapsulation gas is shown as a *filled box*

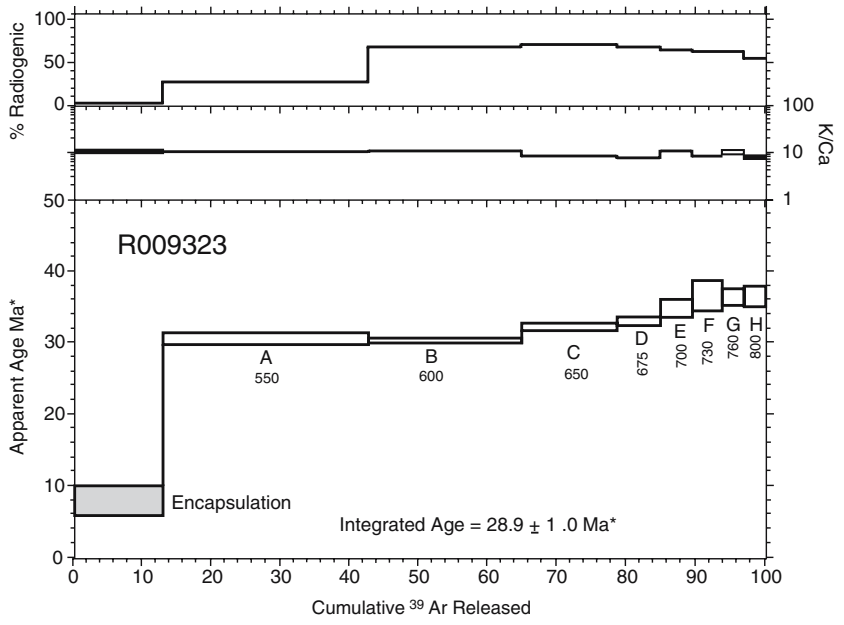

Fig. 8 (continued)

The new model

The data presented are incompatible with the previous models for the origin of the Angouran deposit. We suggest a new model for the genesis of the sulfide ores at Angouran that involves (a) sedimentary brines generated by Miocene seawater evaporation, (b) fluid circulation driven by high geothermal gradients possibly related to the waning stages of Miocene volcanism, (c) metals scavenged from the metamorphic basement and the volcanic rocks, and (d) low-temperature mineralization in marbles within the metamorphic core complex either during a late Miocene extensional or a Plio-Pleistocene compressional regime.

Tectonic evolution and setting

Northeastward subduction of the Neotethys between the Afro-Arabian plate in the southwest and Iranian microplates caused voluminous arc magmatism during the Cretaceous to Eocene (Urumieh-Dokhtar belt) and culminated in continent–continent collision. This caused possibly a regional metamorphic overprint of the Neoproterozoic to Cambrian rock sequence, thrusting and subsequent gentle folding of the crystalline basement in the Angouran region. The Angouran orebody is located in the crest of an open WNW-ESE striking anticline, which is probably related to this Paleogene compressional phase.

During the Oligo-Miocene, a prominent extensional phase followed within the central Sanandaj-Sirjan zone of the Zagros orogenic belt. This extensional phase caused the rapid exhumation of the Neoproterozoic–Cambrian basement in metamorphic core complexes, the formation of intra-arc terrestrial to marine sedimentary basins, and coeval andesitic to rhyolitic igneous activity. Our ^{40}Ar–^{39}Ar muscovite data constrain the timing of rapid exhumation of the basement in the Takab-Zanjan area to the Early Miocene (~20 Ma), consistent with recent apatite U-Th/He data by Stockli et al. (2004) from the Maneshan area a few kilometers north of Angouran, as well as with K–Ar data from a carbonaceous schist in the Zarshuran area (Mehrabi et al. 1999). This relatively late exhumation of the basement also constrains the onset of Neogene sedimentation and volcanic activity in the area and explains the absence of thick continental clastic sediments of the Oligocene Lower Red Formation. Following a short interval of intermediate to acid volcanic to subvolcanic activity with deposition and hydrothermal alteration of rhyolitic pyroclastic rocks, a marine ingression led to the deposition of the Miocene Qom limestones followed by thick continental red beds (Upper Red Formation) with intercalated marine (to lacustrine?) evaporite deposits (gypsum and salt). In the Angouran area, none of the igneous rocks intrude the marine Qom limestones and the overlying Upper Red Formation. In the Zarshuran area, however, andesitic and rhyolitic volcanic rocks with K–Ar and ^{40}Ar–^{39}Ar ages of 16.4±0.3 to 11.1±0.3 Ma (Mehrabi et al. 1999) intrude and overlie sandstones of the Upper Red Fm. Thus, on a more regional scale, Miocene intermediate to acid igneous activity can be considered as approximately coeval with intra-arc marine to continental sedimentation and the generation of evaporative brines, an ingredient required for Zn-(Pb–Ag) mineralization at Angouran. Sedimentary basins with normal geothermal gradients that are sufficiently large and deep (>4 km) to generate brines with temperatures in

excess of 100°C are absent in the Angouran area. We suggest that high regional heat flow, which could be related to the waning stages of extension-related Miocene igneous activity, but which was and is still active during the Quaternary as documented by numerous travertine deposits and active hot springs in the area, was essential for fluid flow and sulfide mineralization at Angouran. Our attempts to precisely date mineralization using the ^{40}Ar–^{39}Ar method on fine-grained ore-related mica failed due to the presence of inherited or excess ^{40}Ar. Thus, the precise timing of ore deposition remains unclear. Sulfide mineralization may be related to the Miocene extensional phase with penetration of evaporative brines into the crystalline basement rocks. Alternatively, westward thrusting of the metamorphic complex onto the Upper Red Formation during the Plio-Pleistocene compressional phase (Stockli et al. 2004) may have been responsible for brine expulsion from the red beds into the hanging wall basement host rocks.

Source of fluids and metals

We suggest that the ore-forming Br-rich Ca–Na–Cl brines are related to the halite-bearing evaporite formation in the Upper Red Formation. The salinity, determined from the microthermometry of the fluid inclusions, the Cl/Br ratios, and the Na and K concentrations in the fluid inclusions are all consistent with the surface evaporation of seawater along the seawater evaporation trend to salinities at which halite precipitates. These dense brines would then have descended into the underlying metamorphic rocks where much of the fluid–rock interaction and leaching of metals would have occurred. We suggest that the fluids only descended to relatively shallow levels as temperatures derived from the chemical geothermometers are only some 70°C higher than the fluid inclusion homogenization temperatures. As this was probably a region of increased heat flow, the fluids probably descended no more than about 1–2 km.

Several other lines of evidence suggest that the brines interacted extensively with the metamorphic rocks prior to ore formation: the Zn-rich nature of the Angouran ores, their high Ni and Co contents (~400 ppm), the presence of excess ^{40}Ar in ore-related micas, the radiogenic Pb isotope composition of ores (cf. Lancelot et al. 1997), and the low Mg content of fluid inclusions. Much of the Zn, Ni, and Co in the ores were most probably leached from the abundant mafic to ultramafic metamorphic rocks in the footwall of the deposit. The relatively high abundance of some other elements such as Ag, Sb, Hg, and As may indicate some contribution of these elements from the Miocene igneous rocks either by leaching with nonmagmatic fluids or less likely by a direct magmatic fluid input. We note here again the overall low contents of Fe (<5 wt%), Cu (<200 ppm), and Au (<10 ppb) in the sulfide ores, which could be taken to indicate the minor involvement of a magmatic component.

Ore-forming mechanism(s)

Our fluid inclusion data exclude fluid phase separation (boiling) and mixing of fluids with variable salinity as ore-forming mechanisms. The location of the sulfide orebody in the lower part of the marbles at the lithological contact with weakly mineralized footwall micaschists strongly suggests that pH changes due to reaction of ascending, probably weakly acid fluids with carbonates played an important role in ore deposition at Angouran. The abundance of angular wall rock breccia fragments within a sulfide ore matrix is conspicuous. The breccia textures are not suggestive of dissolution brecciation as in hydrothermal karsts (e.g., Sass-Gustkiewicz 1996), but are indicative of tectonic or hydraulic brittle fracturing during sulfide deposition (e.g., Borg and Daliran 2004) and possibly seismic pumping of ore fluids. Thus, mineralization may be the result of the transition from a Miocene extensional to a Plio-Pleistocene compressional tectonic regime.

Sulfur was probably initially transported in its oxidized form as sulfate from the evaporite-bearing red beds into the basement rocks. However, sulfate reduction at the site of ore deposition is not considered a likely ore depositional mechanism. The sulfur isotope characteristics and fluid inclusion homogenization data clearly rule out bacterial sulfate reduction (BSR) as the main source for the reduced sulfur in the ores, and rather suggest thermochemical sulfate reduction (TSR). The content of organic carbon, a possible reductant, is too low in the host marbles to account for the large amounts of sulfide ore, and it is unclear if the metamorphosed organic carbon (graphite) was reactive enough to promote TSR. Thus, we suggest that the reduction of sulfate occurred prior to ore deposition as a consequence of reaction of the brines with Fe^{2+}-rich mafic to ultramafic metamorphic rocks, and base metals were finally transported in reduced, acidic brines to their site of deposition. An increase of pH due to reaction of the brines with the marbles and a decrease of temperature may have caused sulfide deposition (e.g. Cooke et al. 2000).

Conclusions

Our study indicates that the Angouran carbonate-hosted Zn–Pb sulfide deposit formed by the interaction of modified Miocene marine evaporation brines with the Neoproterozoic to Cambrian crystalline rocks of an exhumed metamorphic core complex at temperatures of less than 200°C. Mineralization occurred in a collisional intra-arc setting with high tectonic activity and high heat flow, probably during the transition from an extensional to a compressional regime. Minor contributions of metals from the Miocene igneous activity cannot be excluded but appear not to be significant because most of the metals were leached from the metamorphic core complex by evaporative brines. Therefore, the Angouran deposit represents a new type of low-temperature carbonate-hosted Zn–Pb deposit. It is clearly distinct from classical MVT (Leach and Sangster 1993) or

SEDEX deposits (Goodfellow et al. 1993) because epigenetic mineralization at Angouran is hosted within the metamorphic basement and not within sedimentary basins. However, the homogenization temperatures of fluid inclusions (80–160°C) and composition of ore fluids (Ca–Na–Cl brines) at Angouran are similar to those recorded in MVT deposits and indicate that the source and evolution of the ore-forming fluid was broadly similar.

Acknowledgements We are indebted to the Iranian Zinc Mines Development Company (IZMDC), R. Mohammadi Niaei, and S. Modabberi for generous help during field work. M. Sadeghi provided some samples during the early stage of this study. We would like to thank G. Chi (fluid inclusions) and M. Heizler (^{40}Ar–^{39}Ar chronology). Alwyn Annels and Farahnaz Daliran are acknowledged for discussions on the genesis of the Angouran deposits. M. Parente determined the fossils in the Qom limestones. The careful reviews by G. Borg and B. Lehmann are gratefully acknowledged.

References

Alavi M (1994) Tectonics of the Zagros orogenic belt of Iran: new data and interpretation. Tectonophysics 229:211–238

Alinia F (1989) Mineralogy and genesis of Zn–Pb deposit, Anguran, northwest Iran. Abstracts of the 28th International Geological Congress, Washington, DC, (abstract 28/1), p 31

Al Ganad I, Lagny P, Lescuyer JL, Ramboz C, Touray JC (1994) Jabali, a Zn–Pb-(Ag) carbonate-hosted deposit associated with Jurassic rifting in Yemen. Miner Depos 29:44–56

Annels AE, O'Donovan G, Bowles M (2003) New ideas concerning the genesis of the Angouran Zn–Pb deposit, NW Iran. Abstracts of the 26th Mineral Deposits Studies Group, University of Leicester, Leicester, pp 11–12

Asadi HH, Hale M (2001) A predictive GIS model for mapping potential gold and base metal mineralization in Takab area, Iran. Comput Geosci 27:901–912

Asadi HH, Voncken JHL, Hale M, Kuhnel RA (1999) Petrography, mineralogy and geochemistry of the Zarshuran Carlin-like gold deposit. Miner Depos 35:656–671

Babakhani AR, Ghalamghash J (1990) Geological map of Iran, 1:100,000 series sheet Takht-e-Soleiman. Geological Survey of Iran, Tehran

Banks DA, Green R, Cliff RA, Yardley BWD (2000) Chlorine isotopes in fluid inclusions: determination of the origin of salinity in magmatic fluids. Geochim Cosmochim Acta 64:1785–1789

Bariand P, Issakhanian V, Sadrzadeh M (1965) Preliminary metallogenetic map of Iran. Geological Survey of Iran Report No. 7, Tehran, pp 1–50

Böhlke JK, Irwin JJ (1992) Laser microprobe analyses of Cl, Br, I and K in fluid inclusions: implications for sources of salinity in some ancient hydrothermal fluids. Geochim Cosmochim Acta 56:203–225

Borg G, Daliran F (2004) Hypogene and supergene formation of sulphides and non-sulphides at the Angouran high-grade zinc deposit, NW-Iran. In: Abstract volume of Geoscience Africa 2004. University of the Witwatersrand, Johannesburg, pp 69–70

Burnol L (1968) Contribution a l'etude des gisements de plomb et zinc de l'Iran. Essais de classification paragenetique. Geological Survey of Iran Report No. 11, pp 1–113

Cooke DR, Bull SW, Large RR, McGoldrick PJ (2000) The importance of oxidized brines for the formation of Australian Proterozoic stratiform sediment-hosted Pb–Zn (Sedex) deposits. Econ Geol 95:1–18

Daliran F, Borg G (2003) A preliminary appraisal of the non-sulfide zinc deposit of Angouran, north-west Iran. In: Eliopoulos D et al (eds) Mineral exploration and sustainable development. Millpress, Rotterdam, pp 65–68

Daliran F, Borg G (2005) Characterisation of the nonsulfide zinc ore at Angouran, northwestern Iran, and its genetic aspects. In: Jingwen M, Bierlein FP (eds) Mineral deposit research: meeting the global change, vol 2. Springer, Berlin Heidelberg New York, pp 913–916

Daliran F, Hofstra A, Walther J, Stüben D (2002) Agdarreh & Zarshuran SRHDG deposits, Takab region, NW-Iran. Annual meeting of the Geological Society of America, Denver, pp 63–68

Damm B (1968) Geologie des Zendan-i Suleiman und seiner Umgebung südöstliches Balqash-Gebirge Nordwest-Iran. Beiträge zur Archäologie und Geologie des Zendan-i Suleiman, Teil 1. Franz Steiner Verlag, Wiesbaden, pp 1–52

Doe BR, Zartman RE (1979) Plumbotectonics, the Phanerozoic. In: Barnes HL (ed) Geochemistry of hydrothermal ore deposits, 2nd edn. Wiley, New York, pp 22–70

Fontes JC, Matray JM (1993) Geochemistry and origin of formation brines from the Paris Basin, France. 1. Brines associated with Triassic salts. Chem Geol 109:149–175

Gazanfari F (1991) Metamorphic and igneous petrogenesis in NE of Takab with special regard to zinc mineralization in the Angouran mine. Unpubl. Master's thesis, University of Teheran (in Farsi)

Ghazban F, McNutt RH, Schwarcz HP (1994) Genesis of sediment-hosted Zn–Pb–Ba deposits in the Irankuh district, Esfahan area, west-central Iran. Econ Geol 89:1262–1278

Gilg HA (1996) Fluid inclusion and isotope constraints on the genesis of high-temperature carbonate-hosted Pb–Zn–Ag deposits. Society of Economic Geologists Special Publication No. 4, pp 501–514

Gilg HA, Boni M (2004) Stable isotope studies on Zn and Pb carbonates: could they play a role in mineral exploration? In: Pecchio M et al (eds) Applied mineralogy, developments in science and technology, vol 2. ICAM-BR, São Paulo, pp 781–784

Gilg HA, Allen C, Balassone G, Boni M, Moore F (2003) The 3-stage evolution of the Angouran Zn "oxide"-sulfide deposit, Iran. In: Eliopoulos D et al (eds) Mineral exploration and sustainable development. Millpress, Rotterdam, pp 77–80

Glennie KW (2000) Cretaceous tectonic evolution of Arabia's eastern plate margin: a tale of two oceans. In: Middle East models of Jurassic/Cretaceous carbonate systems. SEPM Special Publication No. 69, pp 9–20

Goodfellow WD, Lydon JW, Turner RJW (1993) Geology and genesis of stratiform sediment-hosted (SEDEX) zinc–lead–silver sulfide deposits. In: Kirkham RV, Sinclair WD Thorp RI, Duke JM (eds) Mineral deposit models. Geological Association of Canada Special Paper No. 40, pp 201–252

Grandia F, Canals A, Cardellach E, Banks DA, Perona J (2003) Origin of ore-forming brines in sediment-hosted Zn–Pb deposits of the Basque-Cantabrian basin, Northern Spain. Econ Geol 98:1397–1411

Haditsch JG (1990) Genese der Silizifierung iranischer Blei-Zink-Lagerstaetten. Berg Huettenmann Monatsh 135:197–203

Hamdi B (1995) Precambrian–Cambrian deposits in Iran. In: Hushmandzadeh A (ed) Treatise of the geology of Iran, vol 20. Geological Survey of Iran, Tehran, pp 1–535

Hirayama K (1968) Geological study on the Anguran Mine, northwestern part of Iran. Geological Survey of Japan Report No. 226, pp 1–26

Hitzman MW, Reynolds NA, Sangster DF, Allen CR, Carman CE (2003) Classification, genesis, and exploration guides for nonsulfide zinc deposits. Econ Geol 98:685–714

Houtum-Schindler A (1881) Neue Angaben über die Mineralreichthümer Persiens und über die Gegend westlich von Zendjan. Jb kaiserl kgl Geol Reichsanst 31:169–190

Kharaka YK, Mariner RH (1989) Chemical geothermometers and their application to formation waters from sedimentary basins. In: Naeser ND, McCulloh TH (eds) Thermal history of sedimentary basins. Springer, Berlin Heidelberg New York, pp 99–117

Ladame G (1945) Les ressources métallifères de l'Iran. Schweiz. Mineral Petrogr Mitt 25:165–298

Lancelot J, Orgeval JJ, Fariss K, Zadeh H (1997) Lead isotope signature of major Iranian Zn–Pb ore deposits (Anguran, Duna, Irankuh, Mahdiabad, Nakhlak). Terra Nova 9(Abstr Suppl) 1:550

Leach DL, Sangster DF (1993) Mississippi valley-type lead–zinc deposits. In: Kirkham RV, Sinclair WD, Thorp RI, Duke JM (eds) Mineral deposit models. Geological Association of Canada Special Paper No. 40, pp 289–314

Lotfi M, Karimi M (2004) Geology, mineralogy and ore-genesis of Bayche–Bagh (Ni–Co–As–Bi and base metals) vein-type deposit (NW-Zanjan, Iran). Abstract volume of the 32nd International Geological Congress (part 2, abstract 215-34), p 999

Maanijou M (2002) Proterozoic metallogeny of Iran. Abstracts of the international symposium on the metallogeny of Precambrian shields, Kiev, 13–26 September 2002, p 2

Machel HG, Krouse HR, Sassen R (1995) Products and distinguishing criteria of bacterial and thermochemical sulfate reduction. Appl Geochem 10:373–389

Megaw PKM (1998) Carbonate-hosted Pb–Zn–Ag–Cu–Au replacement deposits: an exploration perspective. In: Lentz DR (ed) Mineralized intrusion-related skarn systems. Mineralogical Association of Canada Short Course Series No. 26, Quebec, pp 337–358

Mehrabi B, Yardley BWD, Cann JR (1999) Sediment-hosted disseminated gold mineralization at Zarshuran, NW Iran. Miner Depos 34:673–696

Minorskij V (1955) Abu-Dulaf Mis'ar Ibn Muhalhil's Travels in Iran, Arabic text with an English translation and commentary. Cairo University Press, Cairo

Naumann E (1961) Geographische und geologische Einordnung. Teheran Forsch 1:15–32

Oakes CS, Bodnar RJ, Simonson JM (1990) The system NaCl-$CaCl_2$-H_2O. I. The ice liquidus at 1 atm total pressure. Geochim Cosmochim Acta 54:603–610

Ohmoto H, Goldhaber MB (1997) Sulfur and carbon isotopes. In: Barnes HL (ed) Geochemistry of hydrothermal ore deposits, 3rd edn. Wiley, New York, pp 517–611

Purdy JW, Jäger E (1976) K–Ar ages on rock-forming minerals from the Central Alps. Mem Ist Geol Mineral Univ Padova 30:1–31

Rahimpour-Bonab H, Kalantarzadeh Z (2005) Origin of secondary potash deposits; a case from Miocene evaporites of NW central Iran. J Asian Earth Sci 25:157–166

Rahimpour-Bonab H, Kazemi H (2003) Geology, mineralogy and genesis of the Gharah-Gol Boron deposit, SW of Zanjan, Iran. J Sci Univ Tehran 29:1–23

Sadeghi M (2003) Mineralogy, geochemistry and fluid inclusion study of Anguran deposit, NW Iran. Abstracts of the 13th V.M. Goldschmidt Conference, Kurashiki, 7–12 September 2003, A406

Sass-Gustkiewicz M (1996) Internal sediments as a key to understanding the hydrothermal karst origin of the Upper Silesian Zn–Pb ore deposits. In: Sangster DF (ed) Carbonate-hosted lead–zinc deposits. Society of Economic Geologists Special Publication No. 4, pp 171–181

Steiger RH, Jäger E (1977) Subcommission on geochronology: convention on the use of decay constants in geo- and cosmochronology. Earth Planet Sci Lett 36:359–362

Stockli DF, Hassanzadeh J, Stockli LD, Axen G, Walker JD, Dewane TJ (2004) Structural and geochronological evidence for Oligo-Miocene intra-arc low-angle detachment faulting in the Takab-Zanjan area, NW Iran. Abstr Programs Geol Soc Am 36(5):319

Velasco F, Herrero JM, Yusta I, Alonso JA, Seebold I, Leach D (2003) Geology and geochemistry of the Reocín zinc–lead deposit, Basque-Cantabrian Basin, Northern Spain. Econ Geol 98:1371–1396

Verma SP, Santoyo E (1997) New improved equation for Na/K, Na/Li and SiO_2 geothermometers by outlier detection and rejection. J Volcanol Geotherm Res 79:9–23

Viets JG, Hofstra AH, Emsbo P (1996) Solute composition of fluid inclusions in sphalerite from North American and European Mississippi-valley type ore deposits: ore fluids derived from evaporated seawater. Society of Economic Geologists Special Publication No. 4, pp 465–482

Walter LM, Stueber AM, Huston TJ (1990) Br–Cl–Na systematics in Illinois basin fluids: constraints on fluid origin and evolution. Geology 18:315–318

Zhang YG, Frantz JD (1987) Determination of the homogenization temperatures and densities of supercritical fluids in the system NaCl-KCl-$CaCl_2$ using synthetic fluid inclusions. Chem Geol 64:335–350